

# 1 Rolling Polyhedra on Tessellations

2 Akira Baes  

3 Département d'Informatique, Université libre de Bruxelles, Belgium.

4 Erik D. Demaine  

5 Computer Science and Artificial Intelligence Laboratory, Massachusetts Institute of Technology,  
6 USA.

7 Martin L. Demaine  

8 Computer Science and Artificial Intelligence Laboratory, Massachusetts Institute of Technology,  
9 USA.

10 Elizabeth Hartung  

11 Department of Mathematics, Massachusetts College of Liberal Arts, USA.

12 Stefan Langerman  

13 Département d'Informatique, Université libre de Bruxelles, Belgium.

14 Joseph O'Rourke  

15 Department of Computer Science, Smith College, Northampton, MA 01063, USA.

16 Ryuhei Uehara  

17 School of Information Science, Japan Advanced Institute of Science and Technology, Japan.

18 Yushi Uno 

19 Graduate School of Informatics, Osaka Metropolitan University, Japan.

20 Aaron Williams  

21 Department of Computer Science, Williams College, USA.

## 22 — Abstract —

23 We study the space reachable by *rolling* a 3D convex polyhedron on a 2D periodic tessellation in  
24 the  $xy$ -plane, where at every step a face of the polyhedron must coincide exactly with a tile of the  
25 tessellation it rests upon, and the polyhedron rotates around one of the incident edges of that face  
26 until the neighboring face hits the  $xy$  plane. If the whole plane can be reached by a sequence of such  
27 rolls, we call the polyhedron a *plane roller* for the given tessellation. We further classify polyhedra  
28 that reach a constant fraction of the plane, an infinite area but vanishing fraction of the plane, or a  
29 bounded area as *hollow-plane rollers*, *band rollers*, and *bounded rollers* respectively. We present a  
30 polynomial-time algorithm to determine the set of tiles in a given periodic tessellation reachable by  
31 a given polyhedron from a given starting position, which in particular determines the roller type  
32 of the polyhedron and tessellation. Using this algorithm, we compute the reachability for every  
33 regular-faced convex polyhedron on every regular-tiled ( $\leq 4$ )-uniform tessellation.

34 **2012 ACM Subject Classification** Theory of computation  $\rightarrow$  Computational geometry; Theory  
35 of computation  $\rightarrow$  Design and analysis of algorithms; Mathematics of computing  $\rightarrow$  Discrete  
36 mathematics

37 **Keywords and phrases** polyhedra, tilings

38 **Digital Object Identifier** 10.4230/LIPIcs.FUN.2022.5

39 **Funding** *Stefan Langerman*: Directeur de Recherches du F.R.S.-FNRS

## 40 **1** Introduction

41 *Dice rolling* puzzles feature a cube rolling around on the square grid. The goal is often to  
42 match a given face with a given tile. Such puzzles were popularized by Martin Gardner  
43 [11, 12, 13], and are featured in a variety of computer games, such as *Korodice* (Gameboy,



© A. Baes, E. D. Demaine, M. L. Demaine, E. Hartung, S. Langerman, J. O'Rourke, R. Uehara, Y. Uno, and A. Williams;

licensed under Creative Commons License CC-BY 4.0

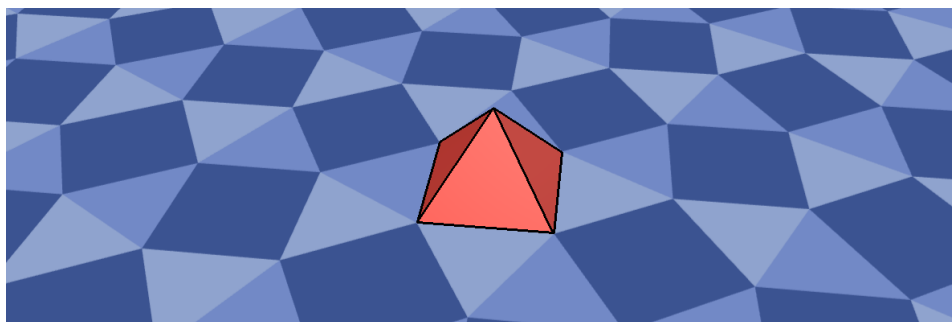
11th International Conference on Fun with Algorithms (FUN 2022).

Editors: Pierre Fraigniaud and Yushi Uno; Article No. 5; pp. 5:1–5:16

Leibniz International Proceedings in Informatics

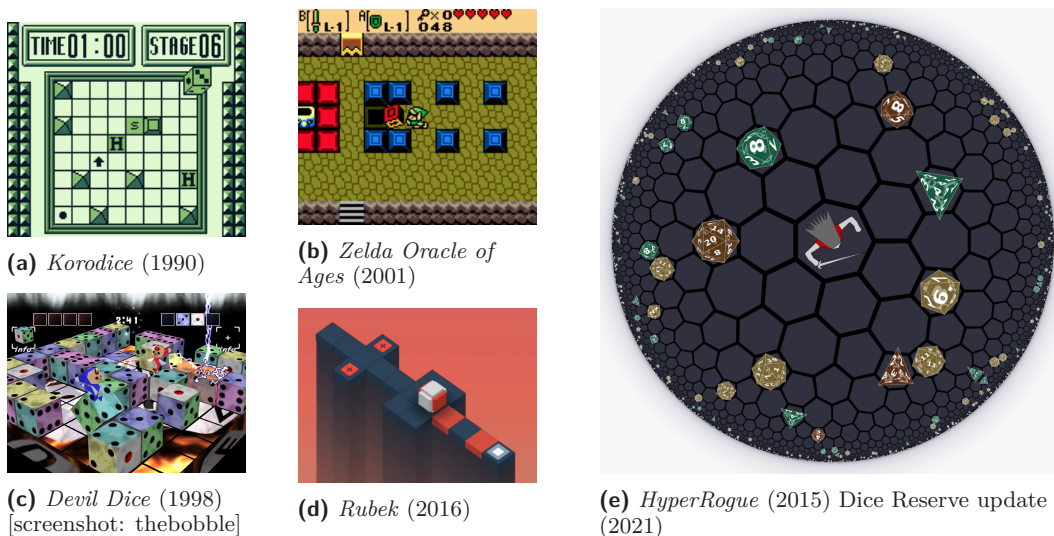


Schloss Dagstuhl – Leibniz-Zentrum für Informatik, Dagstuhl Publishing, Germany



■ **Figure 1** Screenshot from an interactive 3D rolling visualization program on the subject of this paper [3].

44 1990), *Super Mario 64* (Nintendo 64, 1996), *Devil Dice* (Playstation, 1998), *Legacy of*  
 45 *Kain: Soul Reaver* (Playstation, 1999), *Legend of Zelda Oracle of Ages* (Gameboy Color,  
 46 2001), *Bombastic* (Playstation 2, 2002), *Legend of Zelda Spirit Tracks* (Nintendo DS, 2009),  
 47 *Rubek* (Windows, 2016), *Roll The Box* (Mobile, 2021), and *The Last Cube* (Windows,  
 48 2022); see Figure 2. Cube rolling puzzles have been occasionally generalized to rolling  
 49 other polyhedra on other grids. For example, computer game *HyperRogue* (Windows, 2015)  
 50 involves hexagonal and heptagonal tiles in a hyperbolic space, and in its 2021 update, rolling  
 51 tetrahedron, octahedron, or icosahedron dice on a triangular lattice; see Figure 2e. With  
 52 various constraints, rolling puzzles can be NP-complete [6, 18], and when rolling multiple  
 53 shapes, they can be PSPACE-complete [5, 16].

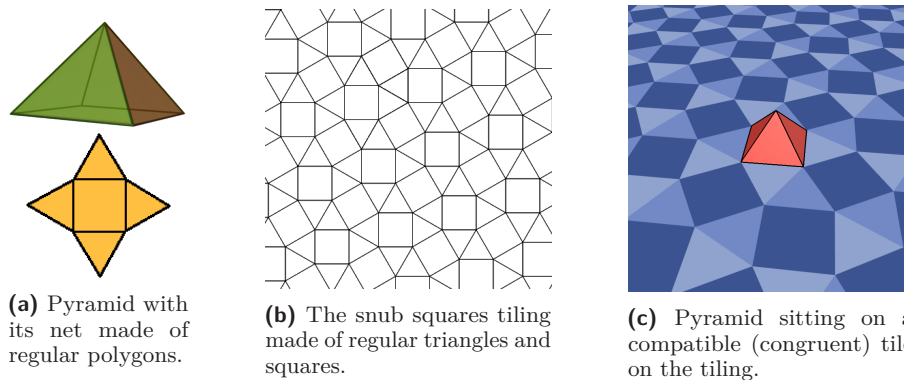


■ **Figure 2** Cube and dice-rolling puzzles in video games.

54 Previous work has explored rolling a polyhedron to reach any position and orientation in  
 55 the plane [8, 4]. Akiyama [1] defined a *frame-stamper* as a regular polyhedron that covers the  
 56 whole plane with a tiling by rolling the polyhedron in arbitrary directions, and a *tile-maker*  
 57 as a polyhedron whose unfoldings all tile the plane. A more relaxed definition in [2] determines  
 58 all *tessellation polyhedra* — regular-faced convex polyhedra that have at least one unfolding  
 59 that tiles the plane.

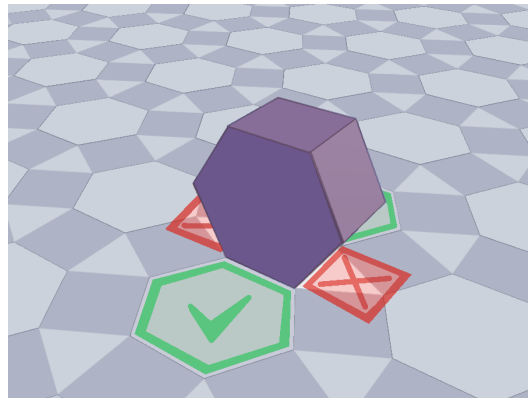
## 60 1.1 Rolling Rollers

61 We formalize the concept of rolling any convex 3D polyhedron  $P$  on any tessellation  $T$ ,  
 62 which we imagine as lying in the (horizontal)  $xy$ -plane; refer to Figure 3. Recall that a  
 63 plane tessellation is a partition of the plane into a collection  $T$  of polygons called *tiles* [15].  
 64 We restrict our attention to *edge-to-edge* tilings where two touching tiles share either a  
 65 whole polygon edge or a vertex. When a tile of  $T$  is congruent to a face of  $P$ , we call them  
 66 *compatible*.



■ **Figure 3** A polyhedron and a tessellation with compatible faces are required for rolling.

67 To start, we place the polyhedron  $P$  on the tessellation so that one of its faces *rests* on  
 68 (i.e., coincides exactly with) a compatible tile. In a *rolling step*, we rotate the polyhedron  
 69 about one of the edges of its resting face, until another face rests on the tessellation. For the  
 70 roll to be *valid*, we insist that, at the end of the motion, the adjacent face of  $P$  across the  
 71 rolling edge rests on another (adjacent) compatible tile. See Figure 4 for an example.



■ **Figure 4** Valid and invalid rolls, marked by green checks and red Xs respectively.

72 Valid sequences of rolls form paths in the *rolling graph* of possible configurations; see  
 73 Section 2.2 for a formal definition. If the rolling graph contains a connected component that  
 74 includes every tile of  $T$ , then we call the polyhedron a *plane roller* (denoted by the 🚲 icon)  
 75 for that tessellation and starting position, as it can eventually roll to cover the entire plane.  
 76 Other possibilities are 🚲 *hollow-plane rollers*, which cover a constant fraction of the plane  
 77 while leaving holes; 🚲 *band rollers*, which cover an infinite area that is a vanishing fraction  
 78 of the plane; and 🚲 *bounded rollers*, which are confined to a finite area.

## 79 1.2 Our Results

80 In this paper, we develop a polynomial-time algorithm to identify whether a polyhedron is a  
 81 plane roller, hollow-plane roller, band roller, or bounded roller for a given plane tessellation and  
 82 starting location, provided the tessellation is *periodic* meaning that its tiles have two linearly  
 83 independent translational symmetries. The running time of our algorithm is polynomial in  
 84 the number of faces of the polyhedron and the number of tiles in the fundamental domain of  
 85 the the two translational symmetries. We essentially take advantage of the periodicity of the  
 86 tessellation, coupled with the structure of the polyhedron, to prove that the resulting rolling  
 87 graph also has a periodic structure that we can exploit.

88 We then apply this algorithm to completely categorize a natural finite set of interesting  
 89 special cases, compiled on the website <https://akirabaes.com/polyrollly/resulttable/>  
 90 shown in Figure 5. For polyhedra, we consider the *regular-faced* convex polyhedra where every  
 91 face is a regular polygon: the 5 Platonic solids [9], the 13 Archimedean solids [10], the 92  
 92 Johnson solids and their chiral variations [14, 17, 19], the  $n$ -prisms for  $n \in \{3, 5, 6, 8, 10, 12\}$ ,  
 93 and the  $n$ -antiprisms for  $n \in \{4, 5, 6, 8, 10, 12\}$ , as higher-sided polygons cannot be used to  
 94 tile the plane [15]. For periodic plane tessellations, we consider all “ $k$ -uniform” tilings for  
 95  $k \geq 4$ , as listed in [7]. A plane tessellation is *k-uniform* if its tiles are regular polygons and it  
 96 is *k-isogonal*, meaning that there are  $k$  equivalence classes of vertices (called *orbits*) formed  
 97 by applying all transformations in the symmetry group to the vertices. All  $k$ -uniform tilings  
 98 are periodic [15].



■ **Figure 5** Screenshot of the rolling-pair reachable-area classification interactive table available at <https://akirabaes.com/polyrollly/resulttable/>.

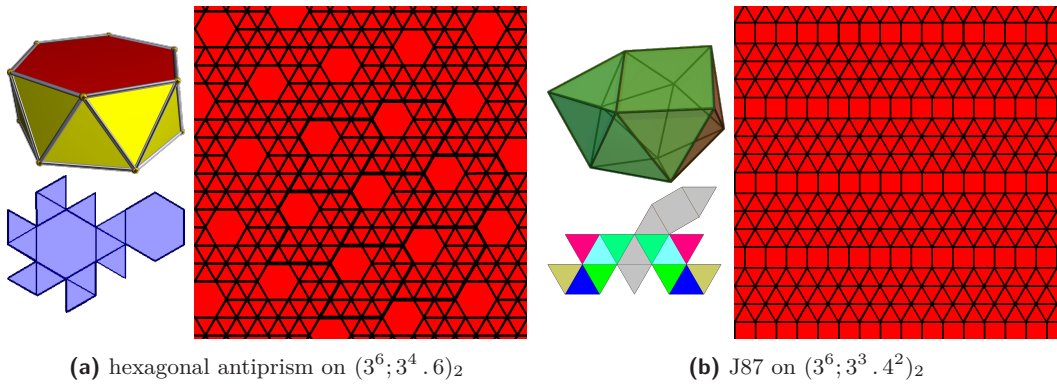



Figure 6 Examples of reachable-area patterns generated by  plane rollers which can reach the entire plane.

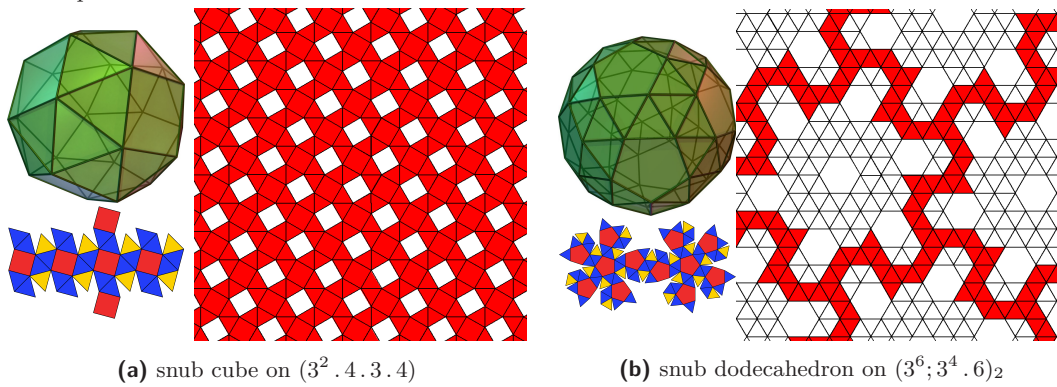



Figure 7 Examples of reachable area patterns generated by  hollow-plane rollers which reach a constant fraction of the plane while leaving holes.

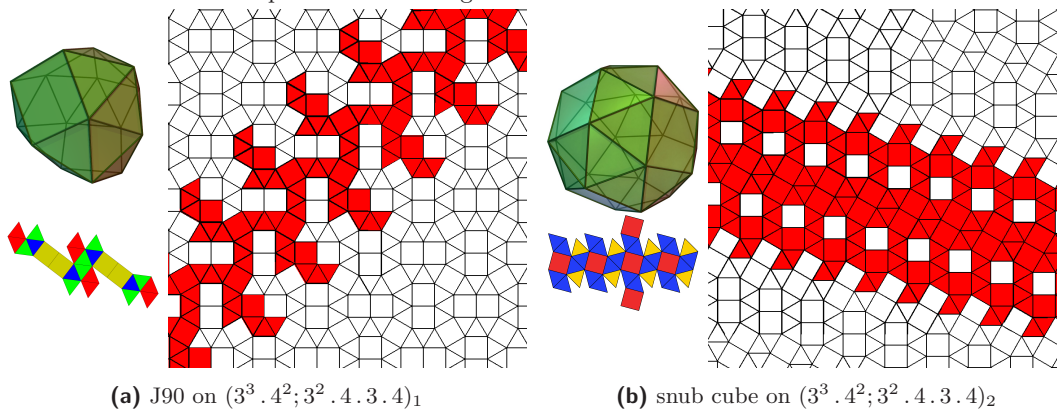





Figure 8 Examples of reachable areas patterns generated by  band rollers which reach an infinite area but a vanishing fraction of the plane, being restricted to an infinite band.

99 Including chiral variations of polyhedra that have one, these cases consist of 129 polyhedra  
 100 and 131 tilings. For each case, we tried all possible starting positions to find the largest  
 101 connected reachable area, thereby characterizing every pair of polyhedron and tiling as  
 102  plane roller,  hollow-plane roller, band roller, or bounded roller. See Figures 6, 7, 8, and  
 103 9 for examples of each respective type, and Tables 2, 3, and 4 in Appendix A for a condensed  
 104 view of all results.

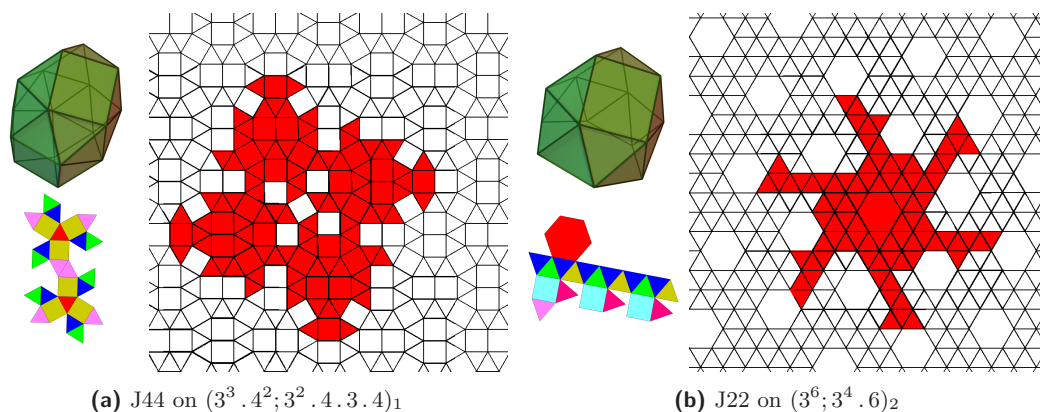


Figure 9 Examples of reachable area patterns generated by  $\blacktriangleright$  bounded rollers which are restricted to a finite area containing the start.

105 The figures and tables use standard notation for  $k$ -uniform tilings based on vertex types  
 106 [7]. The type of a regular-polygon tile is the number of its sides, and the type of a vertex is  
 107 the clockwise cyclic order of tile types that surround a vertex. For a  $k$ -uniform tiling, there  
 108 are finitely many vertex types, so the tiling can be labeled by the list of vertex types, with  
 109 duplicate names differentiated by a subscript. See Figure 10.

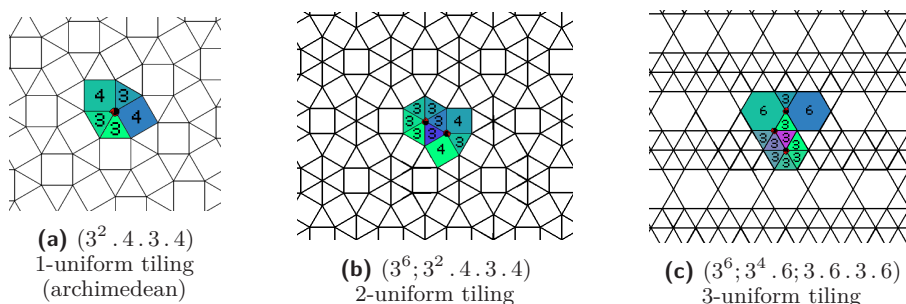


Figure 10 Examples of the naming convention of uniform tilings in the standardized “isogonal vertex type” notation, each point belonging to an orbit describing vertex types around it.

110 The rest of this paper is organized as follows. Section 2 describes our algorithm. Section 3  
 111 shows how the results from this algorithm can also assist puzzle designers. Section 4 describes  
 112 our implementation.

## 2 The Algorithm

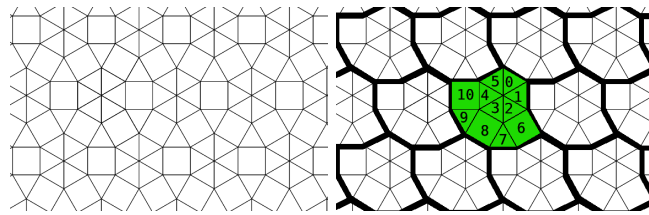
### 2.1 Tilings

115 First we review some basics about tilings, following Grünbaum and Shephard [15].

116 There are uncountably infinitely many tilings, even when restricted to edge-to-edge tilings  
 117 with regular polygons. For example, the tiling in Figure 6b can be modified to follow any  
 118 binary sequence of triangle and square rows, and there are uncountably many such binary  
 119 sequences. We restrict our attention to *periodic tilings*  $T$ , which have two linearly independent  
 120 translational symmetries (say,  $\vec{a}$  and  $\vec{b}$ ) that act on the tiles of  $T$ . What this means is that  
 121 applying the translation vector  $\vec{a}$  (respectively  $\vec{b}$ ) on any tile  $t \in T$  produces another tile of  $T$ .

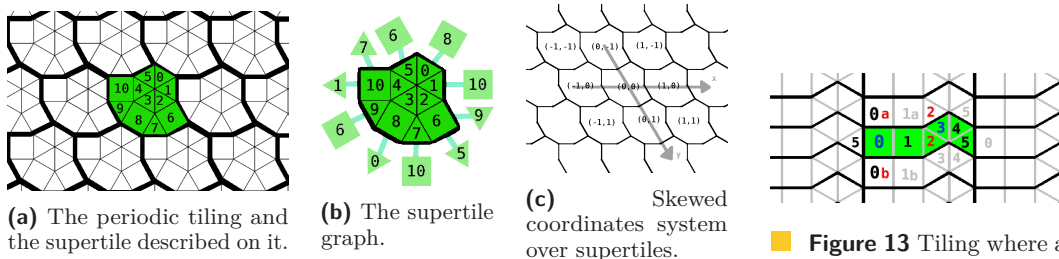
122 The symmetry group generated by  $\vec{a}$  and  $\vec{b}$  decomposes the set of tiles of  $T$  into equivalence  
 123 classes, also called *orbits*, where two tiles are in the same class if there is a symmetry in the  
 124 group (an integer linear combination  $i\vec{a} + j\vec{b}$  for some  $i, j \in \mathbb{Z}$ ) that matches one to the other.

125 The tiling can then be described by a *fundamental domain* for the action of these  
 126 symmetries. Figure 11 shows an example. The fundamental domain is a connected subset of  
 127 the tiles (one tile for each orbit), which glued together form a *supertile*  $S$ . We denote by  $|S|$   
 128 the number of tiles in the supertile. The supertile (and the tiles that compose it) can be  
 129 repeated by the action of the two translations to obtain the original tiling. As  $S$  tiles the  
 130 plane isohedrally by translation, its boundary can be decomposed into six pieces, denoted by  
 131  $A, B, C, \bar{A}, \bar{B}, \bar{C}$ , counterclockwise, where  $\bar{A}, \bar{B}$ , and  $\bar{C}$  are translations of  $A$  by the action of  
 132  $\vec{a}$ ,  $B$  by the action of  $\vec{b}$ , and  $C$  by the action of  $\vec{b} - \vec{a}$ , respectively. See Figure 16 (right).



133 ■ **Figure 11** The same tiling as Figure 10b ( $3^6; 3^2 . 4 . 3 . 4$ ) in its supertile tiling representation.

134 A copy of the supertile can be identified by its integer coordinates in the *basis* formed by  
 135 the translation vectors  $\vec{a}$  and  $\vec{b}$ . That is, the copy  $(i, j)$  corresponds to the application of the  
 136 translation  $i\vec{a} + j\vec{b}$  to  $S$ . An individual tile  $t$  of the tiling  $T$  can then be uniquely identified  
 137 by  $\langle (i, j), s \rangle$ : the coordinates  $(i, j)$  of the copy of  $S$  it is located in and its representative tile  
 $s$  within  $S$ . See Figure 12(a),(c)



(a) The periodic tiling and the supertile described on it.

(b) The supertile graph.

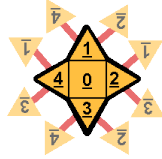
(c) Skewed coordinates system over supertiles.

138 ■ **Figure 13** Tiling where a multigraph is necessary; see tiles 3 and 2.

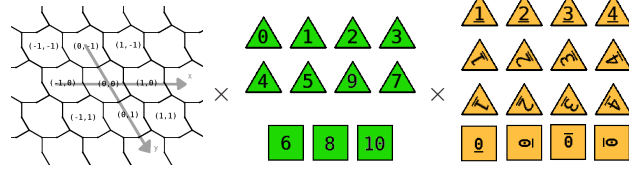
139 ■ **Figure 12** Infinite tiling to supertile multigraph

139 A tiling  $T$  can also be represented by its (infinite) dual graph  $G_T$ ,<sup>1</sup> where each tile is  
 140 a vertex of  $G_T$ , and two vertices are connected by an edge if the two corresponding tiles  
 141 are adjacent. When  $T$  is a periodic tiling, it is represented by the dual multigraph  $G_S$  of  
 142 its supertile  $S$ . For tiles touching the boundary of  $S$ , we connect them to the tiles to which  
 143 they are adjacent in the other copy or copies of the supertile, and mark the dual edges by  
 144  $A, B, C, \bar{A}, \bar{B}$ , or  $\bar{C}$  depending on the portion of the boundary they cross, see Figure 12(b).  
 145 The graph  $G_S$  is in fact the quotient of  $G_T$  by the action of the symmetries  $\vec{a}$  and  $\vec{b}$  (also  
 146 denoted  $G_T / \{\vec{a}, \vec{b}\}$ ). The graph  $G_S$  can be used to navigate the tiling  $T$  or the graph  $G_T$  by  
 updating the representation  $\langle (i, j), s \rangle$  when moving to an adjacent tile. The tile  $s$  is updated

<sup>1</sup> This can be a multigraph, with parallel edges when two tiles are adjacent on more than one edge; see Figure 13.



■ **Figure 14** Dual graph of a pyramid with information about the relative orientations of its faces.



■ **Figure 15** A vertex of the rolling graph is composed of  $\langle(i, j), (tile, face, orientation)\rangle$

147 to the adjacent tile  $s'$  in  $G_S$ , and the coordinates  $(i, j)$  need to be updated when crossing a  
 148 boundary of the supertile  $S$ , using the edge marks.

149 **2.2 Rolling Graphs**

150 Let  $P$  be a convex polyhedron in  $\mathbb{R}^3$ . We denote by  $|P|$  the number of faces of  $P$ . The face  
 151 structure of  $P$  can be represented by its dual graph  $G_P$  where each face of  $P$  is a vertex in  
 152  $G_P$  and two vertices are connected by an edge if the two corresponding faces of  $P$  share an  
 153 edge (Figure 14).

154 For a face  $f \in P$  or a tile  $t \in T$ , denote by  $|f|$  and  $|t|$  its number of edges. We number  
 155 the edges of every face  $f$  of polyhedron  $P$  counter-clockwise starting from one arbitrary edge  
 156 that will serve as the reference edge. We do the same for every tile  $t$  of the supertile  $S$  (and  
 157 the corresponding tessellation  $T$ ), with one edge being the reference edge, and the next edges  
 158 being numbered in clockwise order. A face  $f \in P$  is *compatible* with  $t \in T$  in the *orientation*  
 159  $o$  if  $|f| = |t|$  and the counter-clockwise sequence of edge lengths and angles in  $f$  starting  
 160 at edge number  $o$  matches exactly the clockwise sequence of edge lengths and angles in  $t$   
 161 starting from the reference edge. This means that  $f$  can be placed in the plane with edge  
 162 number  $o$  overlapping with the reference edge of  $t$  so that the two polygons overlap perfectly.

163 We say polyhedron  $P$  *rests on the tile  $t$  in the tessellation  $T$  with its face  $f$  at orientation*  
 164  $o$  if  $f$  and  $t$  completely overlap and the edge number  $o$  of  $f$  overlaps the reference edge of  $t$ .  
 165 The *position* of  $P$  is then represented by the tuple  $\langle t, f, o \rangle$ . When  $T$  is a periodic tiling with  
 166 supertile  $S$ , and  $t = \langle(i, j), s \rangle$  for  $s \in S$ , then this position can be written as  $\langle(i, j), s, f, o \rangle$   
 167 (Figure 15). The *state* associated with this position is the tuple  $\langle s, f, o \rangle$ .

168 The *rolling graph*  $G_{P,T}$  for  $P$  and  $T$  is an infinite graph whose vertex set is the set of all  
 169 possible positions  $\langle t, f, o \rangle$ , and two nodes are connected by an edge if there is a valid roll  
 170 between them. The positions adjacent to  $\langle t, f, o \rangle$  can be easily explored by using the dual  
 171 graphs of  $P$  and  $T$ . We write  $\langle t, f, o \rangle \sim \langle t', f', o' \rangle$  if the two positions are connected by a  
 172 path in the rolling graph. In that case, we say that the two positions are *reachable* from one  
 173 another.

174 **2.3 Symmetries of Rolling Graphs**

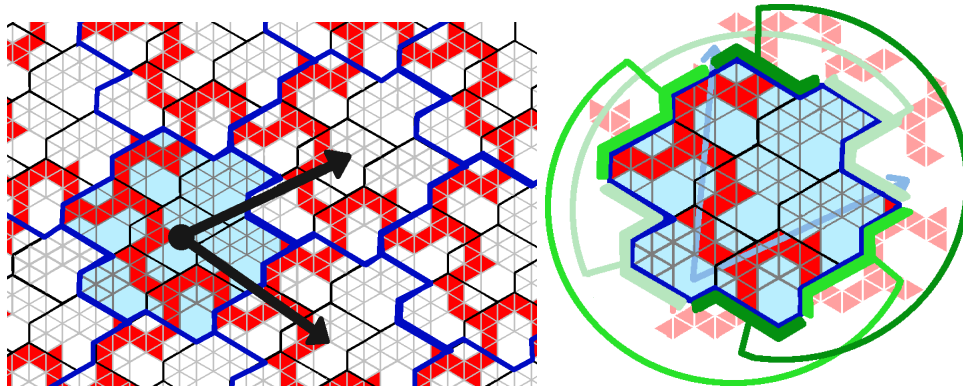
175 In this section, we show that any large connected subgraph of the rolling graph  $G_{P,T}$  has a  
 176 translational symmetry. We start by bounding the number  $N$  of possible states  $\langle s, f, o \rangle$  of a  
 177 rolling graph.

178 
$$N = \sum_{s \in S} \sum_{f \in P} (\text{number of compatible orientations between } f \text{ and } s)$$

179 
$$\leq \sum_{s \in S} \sum_{f \in P} |f| \leq 6|S||P|.$$

180





■ **Figure 16** By finding the symmetry vectors in a connected component, we can describe a compact representation of the connected component's periodic graph (over the rolling graph).

181 The last inequality is by Euler's formula. Note that the rolling graph in itself has the  
 182 same translational symmetries as the tiling  $T$ , because the validity conditions are the same  
 183 in both positions.

184 ► **Fact 1.** *If  $\langle (i, j), s_0, f_0, o_0 \rangle$  has a valid roll to  $\langle (i+i_1, j+j_1), s_1, f_1, o_1 \rangle$ , then  $\langle (i', j'), s_0, f_0, o_0 \rangle$   
 185 has a valid roll to  $\langle (i' + i_0, j' + j_0), s_1, f_1, o_1 \rangle$  for all  $i', j' \in \mathbb{Z}$ .*

186 This however does not mean that the same symmetries apply to the connected components  
 187 of the rolling graph, that is,  $\langle (i, j), s_0, f_0, o_0 \rangle$  and  $\langle (i', j'), s_0, f_0, o_0 \rangle$  might not be reachable,  
 188 even if the connected components are infinite. However, the following lemma shows that if  
 189 two distinct reachable positions have the same state, then we obtain a translational symmetry  
 190 on their connected components in the rolling graph.

191 ► **Lemma 1.** *If  $\langle (i, j), s, f, o \rangle \sim \langle (i + u, j + v), s, f, o \rangle$ , then for all  $\langle (i', j'), s', f', o' \rangle \sim$   
 192  $\langle (i, j), s, f, o \rangle$ , we have  $\langle (i', j'), s', f', o' \rangle \sim \langle (i' + u, j' + v), s', f', o' \rangle$ .*

193 *That is,  $u\vec{a} + v\vec{b}$  defines a translational symmetry on the connected component of  
 194  $\langle (i, j), s, f, o \rangle$  in the rolling graph.*

195 **Proof.** Write the path from  $\langle (i', j'), s', f', o' \rangle$  to  $\langle (i, j), s, f, o \rangle$  in the rolling graph as  $\langle (i, j), s,$   
 196  $f, o \rangle = \langle (i + i_0, j + j_0), s_0, f_0, o_0 \rangle, \dots, \langle (i + i_k, j + j_k), s_k, f_k, o_k \rangle = \langle (i', j'), s', f', o' \rangle$ . Since, by  
 197 Fact 1,  $\langle (i + u + i_\ell, j + u + j_\ell), s_\ell, f_\ell, o_\ell \rangle$  to  $\langle (i + u + i_{\ell+1}, j + u + j_{\ell+1}), s_{\ell+1}, f_{\ell+1}, o_{\ell+1} \rangle$  is a valid  
 198 roll, we can construct the path  $\langle (i', j'), s', f', o' \rangle = \langle (i + i_k, j + j_k), s_k, f_k, o_k \rangle, \dots, \langle (i + i_0, j +$   
 199  $j_0), s_0, f_0, o_0 \rangle = \langle (i, j), s, f, o \rangle \sim \langle (i + u, j + v), s, f, o \rangle = \langle (i + u + i_0, j + v + j_0), s_0, f_0, o_0 \rangle, \dots, \langle (i +$   
 200  $u + i_k, j + v + j_k), s_k, f_k, o_k \rangle = \langle (i' + u, j' + v), s', f', o' \rangle$  ◀

201 ► **Lemma 2.** *There is an algorithm which, in  $O(|P||S|)$  time either finds a base of the  
 202 translational symmetries of the connected component of the rolling graph containing a given  
 203 position  $\langle (i, j), s, f, o \rangle$ , or decides that the connected component is of finite size.*

204 **Proof.** Run a depth first search on the rolling graph starting from  $\langle (i, j), s, f, o \rangle$ , for  $N$  steps.  
 205 If the depth first search stops, then the connected component containing  $\langle (i, j), s, f, o \rangle$  in  
 206 the rolling graph is of finite size. Otherwise, by the pigeonhole principle, we have found two  
 207 positions with the same state. By Lemma 1, we obtain a translational symmetry  $u\vec{a} + v\vec{b}$  of  
 208 the connected component.

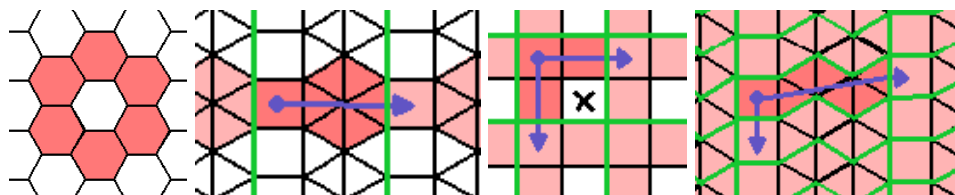
209 Next, factor the rolling graph by this symmetry vector, that is,  $G_{P,T}/\{u\vec{a} + v\vec{b}\}$  identifies  
 210 any pair of positions  $\langle (i, j), s, f, o \rangle$  and  $\langle (i + ku, j + kv), s, f, o \rangle$  for all  $k \in \mathbb{Z}$ . Run again a

211 depth first search in  $G_{P,T}/\{u\vec{a} + v\vec{b}\}$  starting from  $\langle(i, j), s, f, o\rangle$ , for  $N$  steps. If the depth  
 212 first search stops, then there are only a finite number of orbits for this symmetry vector, and  
 213 so only one translational symmetry in this connected component. Otherwise, again by the  
 214 pigeonhole principle and Lemma 1, we have found a second linearly independent translational  
 215 symmetry  $u'\vec{a} + v'\vec{b}$  for this connected component. ◀




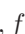
216 The algorithm in the above lemma finds a basis of two, one or zero translational symmetries  
 217 in the connected component. We can factor the rolling graph by those symmetries by  
 218 identifying symmetric tiles. As the symmetries are multiples of the supertile symmetries, this  
 219 is easily done by performing a coordinate change from the  $(i, j)$  coordinates to coordinates  
 220 in the new basis. When there is no symmetry, the algorithm identifies a bounded connected  
 221 component in  $G_{P,T}$ . When there is one symmetry vector, the algorithm finds a finite number  
 222 of orbits for this symmetry. Finally, when there are two symmetry vectors in the basis, the  
 223 factored rolling graph  $G_{P,T}/\{u\vec{a} + v\vec{b}, u'\vec{a} + v'\vec{b}\}$  is of size polynomial in  $N$  and the connected  
 224 component can be explored completely by depth first search. In all three cases, a compact  
 225 representation of the connected component has been found. In the two latter cases, it takes  
 226 the form of a polynomially-sized fundamental domain and one or two translational symmetry  
 227 vectors.

228 **2.3.1 Results on reachability**

229 The arguments above show how to identify the connected components in the rolling graph.  
 230 In order to find the set of tiles that can be reached from a starting position, we only need to  
 231 look at the first part  $(i, j), s$  of the positions in the connected component. Because this is a  
 232 projection, it preserves the symmetry vectors. We obtain the following classification for the  
 233 reachable area.



■ **Figure 17** No vector, one vector, two vectors but fail to cover, two vectors and full cover.

- 234 ■ If the rolling graph does not have symmetry vectors, the reachable area is bounded and  
 235  $P$  on  $T$  starting at  $\langle t, f, o\rangle$ , is a  *bounded roller*.
- 236 ■ If the rolling graph only has one linearly independent vector, the reachable area is a band  
 237 and  $P$  on  $T$  starting at  $\langle t, f, o\rangle$  is a  *band roller*.
- 238 ■ If the rolling graph has two linearly independent vectors, the reachable area extends  
 239 infinitely in all directions. If not every tile  $t$  is present in the reachable supertiles, the  
 240 reachable tiles forms a plane with holes and  $P$  on  $T$  starting at  $\langle t, f, o\rangle$  is a  *hollow-plane*  
 241 *roller*.
- 242 ■ If every tile  $t$  is present in the reachable supertiles, the reachable tiles cover the entire  
 243 plane and  $P$  on  $T$  starting at  $\langle t, f, o\rangle$  is a  *plane roller*.

## 244 **3** Toolbox for Puzzle Designers

245 As mentioned in the Introduction, a rolling puzzle game typically includes a playing area with  
 246 obstacles and/or paths, a polyhedron that will navigate that space, a starting position, and  
 247 a goal position. The starting and/or goal positions sometimes specify a specific polyhedron  
 248 face to match with a specific tile, in addition to just the tile. Once a polyhedron and a  
 249 tessellation have been selected, there are several additional properties that can facilitate  
 250 puzzle design. The rolling graph defined above can also be used to compute them.

### 251 **3.1 Properties**

#### 252 **Unused tiles in the playing area.**

253 The first and most crucial piece of information is provided directly by the reachability  
 254 computed in the previous section. For the puzzle to be solvable, the goal tile should be in  
 255 the reachable area from the start tile. Also, when the game includes interactive elements,  
 256 they cannot not be usefully placed on tiles that cannot be reached (except as misdirection).

#### 257 **Unused faces on the polyhedron.**

258 For face-matching puzzles, determining which faces of the polyhedron are usable in the  
 259 puzzle is also important. Some faces might not be compatible with the tiling, while others  
 260 might not appear in the connected rolling graph despite being compatible. For example,  
 261 puzzle designers should avoid placing the goal on a polyhedron face that cannot be rolled on.  
 262 Unused faces of the polyhedron can easily be detected while computing the reachable area.

#### 263 **Guaranteed starting points.**

264 When using a plane roller, we must select a starting state (tile, face, and orientation) from  
 265 which the polyhedron can reach the whole plane. This task can be simplified by selecting a  
 266 *guaranteed starting point*, which has the property that every tile in the plane is reachable  
 267 from that starting tile, no matter what polyhedron face and orientation is used as a starting  
 268 state.

269 ► **Definition 3.** *Given a plane roller pair  $(P, T)$ , a tile  $t \in T$  is a guaranteed starting point*  
 270 *if, for every  $f \in P$  with  $|f| = |t|$ , and for every  $o \in f$ , we have  $P$  on  $T$  starting at  $\langle t, f, o \rangle$  is*  
 271 *a plane roller.*

272 ► **Definition 4.** *Given a rolling pair  $(P, T)$  with reachable area  $RA$ , a tile  $t \in T$  is a*  
 273 *guaranteed starting point if, for every  $f \in P$  with  $|f| = |t|$ , for every  $o \in f$ , and for every*  
 274  *$t_i \in RA$ , there is a face  $f_i$  and orientation  $o_i$  such that  $\langle t, f, o \rangle \sim \langle t_i, f_i, o_i \rangle$ .*

#### 275 **Which faces reach which tiles: face-completeness.**

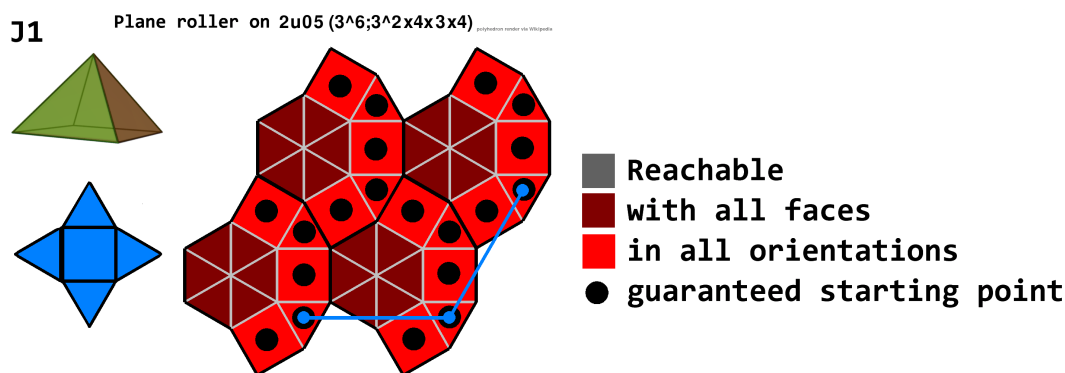
276 In a face-matching rolling puzzle game, the objective is to reach a specific tile with a specific  
 277 face on the polyhedron (often marked by a different color). In some cases, not every face of a  
 278 particular shape can reach every tile. When using a polyhedron/tiling pair in a puzzle game,  
 279 it can help to know which face can reach which tile. We can track specific tiles that can be  
 280 reached by every compatible face during our computation. We call such tiles *face-complete*  
 281 tiles. Refer to Figure 18.

282 ► **Definition 5** (face-complete tile). A rolling pair  $(P, T)$  with starting state  $\langle t_0, f_0, o_0 \rangle$  has  
 283 a face-complete tile  $t \in T$  if all compatible faces of the polyhedron can roll on  $t$  with  
 284 some orientation, that is, for all  $f \in P$  with  $|f| = |t|$ , there is an orientation  $o$  such that  
 285  $\langle t, f, o \rangle \sim \langle t_0, f_0, o_0 \rangle$ .

286 ► **Definition 6** (face-orientation-complete tile). A tile is face-orientation-complete if it can  
 287 be visited with all compatible faces in every orientation within a connected component.

### 288 3.2 Puzzlemaker's Reference Image

289 We can combine all of the above results into one image that serves as a reference point for  
 290 puzzlemakers. Figure 18 shows an example. This image allows one to select a tessellation/  
 291 polyhedron pair very easily depending on the puzzle's needs.



■ **Figure 18** Puzzlemaker's reference image: Left: polyhedron and its used faces (net). Right: Tiling and tile properties.

292 The full set of reference images can be found on our website: <https://akirabaes.com/polyroll/>.  
 293

## 294 4 Implementation

295 The roller classification algorithm was implemented in Python 3.8 and is available on  
 296 GitHub at <https://github.com/akirbaes/RollingPolyhedron/>. It uses NumPy and  
 297 SymPy for creating a minimal linearly independent base, and pygame to produce images. The  
 298 implemented version performs further manipulations, such as aggregating connected rolling  
 299 graph states grouped by supertile into superstates, to lower processing time and avoid dealing  
 300 with individual tile positions calculations by only looking at the supertile cartesian coordinates.  
 301 The result table can be consulted at <https://akirabaes.com/polyroll/resulttable/>.

302 We defined the supertiles of each tiling by hand in a custom periodic tessellation drawing  
 303 tool, as we lacked code to automatically convert vertex-type orbits (isohedral, edges) notation  
 304 to dual-graph supertile (isogonal, tiles) notation, but we did have a list of  $n$ -uniform  
 305 tessellation drawings [7].

306 An interactive 3D visualization of the rolling logic was implemented by Université libre  
 307 de Bruxelles Computer Science Bachelor students [3]; see Figure 1.

## 5 Open Problem

It is left to determine, for the 87 polyhedra out of the 129 considered that did not generate a plane roller with the 131 considered tilings, if there exists a tiling on which they would be able to roll on the 2D plane.

dodecahedron, truncated cube, truncated octahedron, rhombicuboctahedron, truncated cuboctahedron, snub cube, snub cube c, icosidodecahedron, truncated dodecahedron, truncated icosahedron, rhombicosidodecahedron, truncated icosidodecahedron, snub dodecahedron, snub dodecahedron c, j2, j4, j5, j6, j7, j9, j18, j19, j20, j21, j23, j24, j25, j32, j33, j34, j35, j36, j38, j39, j40, j41, j42, j43, j45, j45 c, j46, j46 c, j47, j47 c, j48, j48 c, j49, j52, j53, j55, j57, j58, j59, j60, j61, j63, j64, j66, j67, j68, j69, j70, j71, j72, j73, j74, j75, j76, j77, j78, j79, j80, j81, j82, j83, j91, j92, triangular prism, pentagonal prism, hexagonal prism, octagonal prism, decagonal prism, dodecagonal prism, pentagonal antiprism, octagonal antiprism, decagonal antiprism, dodecagonal antiprism

■ **Table 1** Considered polyhedra which did not generate a plane roller with considered tilings

## Acknowledgements

Part of this work appeared in the first author's Master's Thesis. Part of this work was done at the 1st and 2nd Virtual Workshops on Computational Geometry (2020 and 2021). The authors would like to thank all participants of those workshops. Renders of prisms and antiprisms are by Robert Webb's Stella software. Other polyhedron renders are from Wikimedia Commons under Creative Commons Attribution license.

## References

- 1 Jin Akiyama. Tile-makers and semi-tile-makers. *The American Mathematical Monthly*, 114(7):602–609, 2007.
- 2 Jin Akiyama, Takayasu Kuwata, Stefan Langerman, Kenji Okawa, Ikuro Sato, and Geoffrey C. Shephard. Determination of all tessellation polyhedra with regular polygonal faces. In *International Conference on Computational Geometry, Graphs and Applications*, pages 1–11, 2010.
- 3 Rachel Aouad Albashara, Luca Insisa, Quentin Magron, Dan Ngongo, Dang Phi L Pham, and Simon Yousfi. Rouler des polyèdres sur des tessellations. Université libre de Bruxelles Computer Science Bachelor *Printemps des Sciences* showcase, 2022. <https://akirabaes.com/polyroll/printempsdesciences2022>.
- 4 Antonio Bicchi, Yacine Chitour, and Alessia Marigo. Reachability and steering of rolling polyhedra: a case study in discrete nonholonomy. *IEEE Transactions on Automatic Control*, 49(5):710–726, 2004.
- 5 Kevin Buchin and Maike Buchin. Rolling block mazes are pspace-complete. *Journal of Information Processing*, 20(3):719–722, 2012. doi:10.2197/ipsjjip.20.719.
- 6 Kevin Buchin, Maike Buchin, Erik D. Demaine, Martin L. Demaine, Dania El-Khechen, Sándor Fekete, Christian Knauer, André Schulz, and Perouz Taslakian. On rolling cube puzzles. In *Proceedings of the 19th Canadian Conference on Computational Geometry (CCCG 2007)*, Ottawa, Canada, August 2007.

## 5:14 Rolling Polyhedra on Tessellations

- 338 7 D. Chavey. Tilings by regular polygons—II: A catalog of tilings. *Computers & Mathematics*  
339 *with Applications*, 17(1–3):147–165, 1989.
- 340 8 Yacine Chitour, Alessia Marigo, Domenico Prattichizzo, and Antonio Bicchi. Rolling polyhedra  
341 on a plane, analysis of the reachable set. In *Algorithms for Robotic Motion and Manipulation*  
342 *(WAFR 1996)*, pages 277–285. 1997.
- 343 9 Euclid. *Elements*, volume I. Circa 300 BCE.
- 344 10 Judith V. Field. Rediscovering the archimedean polyhedra: Piero della francesca, luca Pacioli,  
345 leonardo da vinci, albrecht dürer, daniele barbaro, and johannes kepler. *Archive for History of*  
346 *Exact Sciences*, 50(3/4):241–289, 1997.
- 347 11 Martin Gardner. *Martin Gardner’s Sixth Book of Mathematical Diversions from Scientific*  
348 *American*. W H Freeman, San Francisco, 1971. Chapter 8.
- 349 12 Martin Gardner. *Mathematical Carnival*. Borzoi / Alfred A Knopf, New York, 1975. Chapter  
350 9, Problem 1: The red-faced cube.
- 351 13 Martin Gardner. *Time Travel and Other Mathematical Bewilderments*. W H Freeman, New  
352 York, 1988. Chapter 9, Problem 8: Rolling cubes.
- 353 14 B. Grünbaum and N. W. Johnson. The faces of a regular-faced polyhedron. *Journal of the*  
354 *London Mathematical Society*, 1(1):577–586, 1965.
- 355 15 Branko Grünbaum and G. C. Shephard. *Tilings and Patterns*. W. H. Freeman and Company,  
356 1987.
- 357 16 Markus Holzer and Sebastian Jakobi. On the complexity of rolling block and Alice mazes. In  
358 *Proceedings of the 6th International Conference on Fun with Algorithms*, pages 210–222, 2012.
- 359 17 Norman W Johnson. Convex polyhedra with regular faces. *Canadian Journal of Mathematics*,  
360 18:169–200, 1966.
- 361 18 Akihiro Uejima and Takahiro Okada. NP-completeness of rolling dice puzzles using octahedral  
362 and icosahedral dices (in Japanese). *IEICE Trans. Fund.*, J94-A(8):621–628, 2011.
- 363 19 Viktor Abramovich Zalgaller. Convex polyhedra with regular faces. *Zapiski Nauchnykh*  
364 *Seminarov POMI*, 2:5–221, 1967.

## A

 Result Tables

**tetrahedron** with  $(3^6)$  • **cube** with  $(4^4)$  • **octahedron** with  $(3^6)$  • **icosahedron** with  $(3^6)$  • **truncated tetrahedron** with  $(3^6; 3^2.6^2)$  • **cuboctahedron** with  $(3^2.4.3.4)$ ,  $(3^6; 3^2.4.3.4)$ ,  $(3^3.4^2; 3^2.4.3.4)1$ ,  $(3^6; 3^2.4.3.4; 3^2.4.3.4)$  • **j1** with  $(3^2.4.3.4)$ ,  $(3^6; 3^2.4.3.4)$ ,  $(3^3.4^2; 3^2.4.3.4)1$ ,  $(3^6; 3^3.4^2; 3^2.4.3.4)$ ,  $(3^6; 3^2.4.3.4; 3^2.4.3.4)$  • **j3** with  $(3^6; 3^2.4.3.3.4; 3.4^2.6)$ ,  $(3^6; 3^2.4.3.4; 3.4^2.6; 3.4.6.4)$  • **j8** with  $(4^4)$ ,  $(3^6; 3^3.4^2; 4^4)1$ ,  $(3^6; 3^3.4^2; 4^4)3$ ,  $(3^6; 3^3.4^2; 3^2.4.3.4; 4^4)$  • **j10** with  $(3^6)$ ,  $(3^6; 3^3.4^2)1$ ,  $(3^6; 3^3.4^2)2$ ,  $(3^6; 3^2.4.3.4)$ ,  $(3^6; 3^3.4^2; 3^2.4.3.4)$ ,  $(3^6; 3^6; 3^3.4^2)1$ ,  $(3^6; 3^6; 3^3.4^2)2$ ,  $(3^6; 3^3.4^2; 3^2.4.3.4; 4^4)$  • **j11** with  $(3^6)$  • **j12** with  $(3^6)$  • **j13** with  $(3^6)$  • **j14** with  $(3^6; 3^3.4^2)1$  • **j15** with  $(3^6; 3^3.4^2)1$  • **j16** with  $(3^6; 3^3.4^2)1$  • **j17** with  $(3^6)$  • **j22** with  $(3^6; 3^4.6)1$ ,  $(3^6; 3^4.6; 3.6.3.6)2$ ,  $(3^6; 3^4.6; 3.6.3.6)3$ ,  $(3^6; 3^6; 3^4.6^2)$  • **j26** with  $(3^2.4.3.4)$ ,  $(3^3.4^2; 3^2.4.3.4)2$ ,  $(3^6; 3^2.4.3.4; 3^2.4.3.4)$  • **j27** with  $(3^3.4^2)$ ,  $(3^3.4^2; 3^2.4.3.4)1$ ,  $(3^6; 3^3.4^2; 3^2.4.3.4)$ ,  $(3^3.4^2; 3^2.4.3.4; 3^2.4.3.4)$  • **j28** with  $(3^3.4^2)$ ,  $(3^3.4^2; 4^4; 4^4)1$  • **j29** with  $(3^2.4.3.4)$ ,  $(3^6; 3^2.4.3.4; 3^2.4.3.4)$  • **j30** with  $(3^3.4^2)$  • **j31** with  $(3^2.4.3.4)$ ,  $(3^6; 3^2.4.3.4; 3^2.4.3.4)$  • **j37** with  $(4^4)$  • **j44** with  $(3^6; 3^2.4.3.4; 3^2.4.3.4)$ ,  $(3^3.4^2; 3^2.4.3.4; 3^2.4.3.4)$  • **j44 chiral** with  $(3^6; 3^2.4.3.4; 3^2.4.3.4)$  • **j50** with  $(3^6)$ ,  $(3^6; 3^3.4^2)1$ ,  $(3^6; 3^3.4^2)2$ ,  $(3^6; 3^2.4.3.4)$ ,  $(3^6; 3^6; 3^3.4^2)1$ ,  $(3^6; 3^6; 3^3.4^2)2$ ,  $(3^6; 3^3.4^2; 3^2.4.3.4; 4^4)$  • **j51** with  $(3^6)$  • **j54** with  $(3.4.6.4)$  • **j56** with  $(3.4.6.4)$  • **j62** with  $(3^6)$  • **j65** with  $(3.6.3.6)$  • **j84** with  $(3^6)$  • **j85** with  $(3^6)$ ,  $(3^6; 3^3.4^2)1$ ,  $(3^6; 3^3.4^2)2$ ,  $(3^6; 3^2.4.3.4)$ ,  $(3^6; 3^6; 3^3.4^2)1$ ,  $(3^6; 3^6; 3^3.4^2)2$ ,  $(3^6; 3^3.4^2; 3^3.4^2)1$ ,  $(3^6; 3^3.4^2; 3^3.4^2)2$ ,  $(3^6; 3^3.4^2; 3^2.4.3.4; 4^4)$  • **j86** with  $(3^6)$ ,  $(3^6; 3^3.4^2)1$ ,  $(3^6; 3^3.4^2)2$ ,  $(3^6; 3^2.4.3.4)$ ,  $(3^6; 3^3.4^2; 3^2.4.3.4)$ ,  $(3^6; 3^3.4^2; 4^4)1$ ,  $(3^6; 3^3.4^2; 4^4)2$ ,  $(3^6; 3^6; 3^3.4^2)1$ ,  $(3^6; 3^6; 3^3.4^2)2$ ,  $(3^6; 3^3.4^2; 3^2.4.3.4; 4^4)$  • **j87** with  $(3^6)$ ,  $(3^6; 3^3.4^2)1$ ,  $(3^6; 3^3.4^2)2$ ,  $(3^6; 3^2.4.3.4)$ ,  $(3^6; 3^6; 3^3.4^2)1$ ,  $(3^6; 3^6; 3^3.4^2)2$ ,  $(3^6; 3^3.4^2; 3^2.4.3.4; 4^4)$  • **j88** with  $(3^6)$ ,  $(3^6; 3^3.4^2)1$ ,  $(3^6; 3^3.4^2)2$ ,  $(3^6; 3^3.4^2; 3^2.4.3.4)$ ,  $(3^6; 3^3.4^2; 4^4)1$ ,  $(3^6; 3^3.4^2; 4^4)2$ ,  $(3^6; 3^6; 3^3.4^2)1$ ,  $(3^6; 3^6; 3^3.4^2)2$ ,  $(3^6; 3^3.4^2; 3^3.4^2)1$ ,  $(3^6; 3^3.4^2; 3^3.4^2)2$  • **j89** with  $(3^6)$ ,  $(3^6; 3^3.4^2)1$ ,  $(3^6; 3^3.4^2)2$ ,  $(3^6; 3^2.4.3.4)$ ,  $(3^6; 3^3.4^2; 3^2.4.3.4)$ ,  $(3^6; 3^3.4^2; 4^4)3$ ,  $(3^6; 3^3.4^2; 4^4)4$ ,  $(3^6; 3^6; 3^3.4^2)1$ ,  $(3^6; 3^6; 3^3.4^2)2$ ,  $(3^6; 3^3.4^2; 3^3.4^2)1$ ,  $(3^6; 3^3.4^2; 3^3.4^2)2$  • **j90** with  $(3^6)$ ,  $(3^6; 3^3.4^2)1$ ,  $(3^6; 3^3.4^2)2$ ,  $(3^6; 3^2.4.3.4)$ ,  $(3^6; 3^3.4^2; 3^2.4.3.4)$ ,  $(3^6; 3^3.4^2; 4^4)1$ ,  $(3^6; 3^3.4^2; 4^4)2$ ,  $(3^6; 3^6; 3^3.4^2)1$ ,  $(3^6; 3^6; 3^3.4^2)2$ ,  $(3^6; 3^3.4^2; 3^3.4^2)1$ ,  $(3^6; 3^3.4^2; 3^3.4^2)2$ ,  $(3^6; 3^2.4.3.4; 3^2.4.3.4)$ ,  $(3^6; 3^3.4^2; 3^2.4.3.4; 4^4)$  • **square antiprism** with  $(3^3.4^2)$  • **hexagonal antiprism** with  $(3^4.6)$ ,  $(3^6; 3^4.6)1$ ,  $(3^6; 3^4.6)2$ ,  $(3^4.6; 3^2.6^2)$ ,  $(3^6; 3^4.6; 3^2.6^2)2$ ,  $(3^6; 3^4.6; 3.6.3.6)1$ ,  $(3^6; 3^4.6; 3.6.3.6)2$ ,  $(3^6; 3^4.6; 3.6.3.6)3$ ,  $(3^6; 3^6; 3^4.6^2)$ ,  $(3^6; 3^4.6; 3^4.6)$ ,  $(3^4.6; 3^4.6; 3.6.3.6)1$ ,  $(3^4.6; 3^4.6; 3.6.3.6)2$ ,  $(3^6; 3^4.6; 3^2.6^2; 3.6.3.6)$ ,  $(3^4.6; 3^2.6^2; 3^2.6^2; 3.6.3.6)$

■ **Table 2**  Plane-roller polyhedra and tilings (42 polyhedra and 145 pairings).

tetrahedron (x7) • octahedron (x7) • icosahedron (x7) • truncated tetrahedron (x12) • cuboctahedron (x4) • truncated cube • truncated octahedron (x10) • rhombicuboctahedron (x8) • truncated cuboctahedron (x6) • snub cube (x13) • snub cube chiral (x12) • truncated icosahedron (x4) • rhombicosidodecahedron (x4) • truncated icosidodecahedron (x5) • snub dodecahedron (x5) • snub dodecahedron chiral (x4) • j1 (x6) • j3 (x8) • j7 (x5) • j8 • j10 (x15) • j11 (x6) • j12 (x7) • j13 (x7) • j14 (x15) • j15 (x15) • j16 (x15) • j17 (x7) • j18 (x7) • j19 (x4) • j22 • j26 (x2) • j27 (x13) • j28 (x8) • j29 (x2) • j30 (x6) • j31 • j35 (x11) • j37 (x3) • j38 (x7) • j44 (x6) • j44 chiral (x5) • j45 (x2) • j45 chiral (x2) • j49 (x8) • j50 (x16) • j51 (x7) • j53 (x6) • j54 (x14) • j55 (x10) • j56 (x16) • j57 (x14) • j62 (x4) • j65 (x3) • j66 • j72 (x4) • j74 (x10) • j75 (x6) • j76 (x4) • j78 (x4) • j79 (x6) • j81 (x4) • j84 (x7) • j85 (x16) • j86 (x16) • j87 (x18) • j88 (x18) • j89 (x20) • j90 (x16) • triangular prism (x12) • hexagonal prism (x18) • octagonal prism • dodecagonal prism (x4) • square antiprism (x5) • hexagonal antiprism (x2) • dodecagonal antiprism (x2)

■ **Table 3** 🧩 Hollow-plane-roller polyhedra and tilings (76 polyhedra and 588 pairings).

tetrahedron (x35) • cube (x41) • octahedron (x35) • icosahedron (x35) • truncated tetrahedron (x34) • cuboctahedron (x3) • truncated octahedron (x15) • rhombicuboctahedron (x43) • snub cube (x7) • snub cube chiral (x8) • truncated icosahedron (x13) • rhombicosidodecahedron (x2) • snub dodecahedron (x7) • snub dodecahedron chiral (x7) • j1 (x7) • j3 (x2) • j7 (x43) • j8 (x39) • j9 (x42) • j10 (x29) • j11 (x31) • j12 (x35) • j13 (x35) • j14 (x42) • j15 (x42) • j16 (x42) • j17 (x35) • j18 (x43) • j19 (x41) • j20 (x42) • j21 (x42) • j22 (x30) • j23 (x30) • j24 (x30) • j25 (x30) • j26 (x7) • j27 (x17) • j28 (x46) • j29 (x4) • j30 (x15) • j31 (x3) • j35 (x44) • j36 (x49) • j37 (x46) • j38 (x44) • j39 (x47) • j40 (x42) • j41 (x42) • j42 (x42) • j43 (x42) • j44 (x32) • j44 chiral (x33) • j45 (x31) • j45 chiral (x32) • j46 (x32) • j46 chiral (x32) • j47 (x30) • j47 chiral (x30) • j48 (x30) • j48 chiral (x30) • j49 (x20) • j50 (x27) • j51 (x35) • j54 (x8) • j55 (x10) • j56 (x15) • j57 (x11) • j62 (x17) • j65 (x25) • j67 • j72 • j73 (x5) • j76 • j77 (x5) • j80 (x5) • j84 (x35) • j85 (x32) • j86 (x27) • j87 (x28) • j88 (x23) • j89 (x21) • j90 (x25) • triangular prism (x45) • pentagonal prism (x42) • hexagonal prism (x36) • octagonal prism (x42) • decagonal prism (x42) • dodecagonal prism (x43) • square antiprism (x37) • pentagonal antiprism (x30) • hexagonal antiprism (x40) • octagonal antiprism (x30) • decagonal antiprism (x30) • dodecagonal antiprism (x30)

■ **Table 4** 🧩 Band-roller polyhedra and tilings (94 polyhedra and 2623 pairings).